



**HAL**  
open science

# The effect of pore geometry in constitutive hysteretic models for unsaturated water flow

Mariangeles Soldi, Luis Guarracino, Damien Jougnot

## ► To cite this version:

Mariangeles Soldi, Luis Guarracino, Damien Jougnot. The effect of pore geometry in constitutive hysteretic models for unsaturated water flow. *Environmental Fluid Mechanics*, 2022, <10.1007/s10652-022-09891-0>. <hal-03758111>

**HAL Id: hal-03758111**

**<https://hal.sorbonne-universite.fr/hal-03758111v1>**

Submitted on 22 Aug 2022

HAL is a multi-disciplinary open access archive for the deposit and dissemination of scientific research documents, whether they are published or not. The documents may come from teaching and research institutions in France or abroad, or from public or private research centers.

L'archive ouverte pluridisciplinaire HAL, est destinée au dépôt et à la diffusion de documents scientifiques de niveau recherche, publiés ou non, émanant des établissements d'enseignement et de recherche français ou étrangers, des laboratoires publics ou privés.



HAL Authorization

# The effect of pore geometry in constitutive hysteretic models for unsaturated water flow

M. Soldi<sup>1\*</sup>, L. Guarracino<sup>1</sup> and D. Jougnot<sup>2</sup>

<sup>1</sup>Facultad de Ciencias Astronómicas y Geofísicas, Universidad Nacional de La Plata, Consejo Nacional de Investigaciones Científicas y Técnicas, La Plata, Argentina

<sup>2</sup>Sorbonne Université, CNRS, EPHE, UMR 7619 METIS, 75005, Paris, France

\*E-mail: msoldi@fcaglp.unlp.edu.ar

This paper has been published in Environmental Fluid Mechanics:  
Soldi, M., Guarracino, L. and Jougnot, D. (2022) The effect of pore geometry in constitutive hysteretic models for unsaturated water flow. Environmental Fluid Mechanics.  
<https://doi.org/10.1007/s10652-022-09891-0>

## Abstract

Water flow in porous media is strongly controlled by the microscale structure of the pore space. Therefore, understanding the dynamics at pore scale is fundamental to better estimate and describe the hydraulic properties and phenomena associated to water flow which are observed in a macroscale such as field or laboratory experiments. Pore geometry plays a key role since its variations cause modifications in hydraulic behaviour at the macroscale. In this study, we develop a new analytical model which represents the pore space of a medium as a bundle of tortuous sinusoidal capillary tubes with periodic pore throats and a fractal pore-size distribution. This model is compared with a previous model of straight constrictive capillary tubes in order to analyze the effect of pore geometry on hydraulic properties under partially saturated conditions. The comparison of the constitutive models shows that macroscopic hydraulic properties, porosity and permeability, present the strongest differences due to changes in the pore geometry. Nonetheless, no variations are observed in the relative hydraulic properties, effective saturation and relative permeability. The new model has been tested with experimental data consisting on sets of porosity-permeability, water content-pressure head, conductivity-pressure head, and hysteretic water content-pressure values. In all cases, the model is able to satisfactorily reproduce the data. This new analytical model presents an improvement over the previous model since the smoother variation of the pore radii allows a more realistic representation of the porous medium.

## Article Highlights

- New constitutive model to describe hydraulic properties of porous media.
- Variations in pore geometry significantly influence porosity and permeability estimates.
- The physically-based model has analytical closed-form expressions whose predictions are consistent with laboratory data.

Keywords: Hydraulic Properties, Pore geometry, Hysteresis, Vadose Zone

# 1 Introduction

Flow and transport properties observed and measured in field or laboratory experiments are significantly influenced by the structure of porous media at the microscale. The pore space structure in which water flow occurs can be extremely irregular and complex for a real porous medium and plays a key role in the description of those hydraulic properties. In fact, the irregularities within the pore structure (i.e. constrictivities of the pore space) produce the hysteresis phenomenon in the hydraulic properties under unsaturated conditions of the medium (e.g. Bear, 1998; Vogel and Roth, 2001). Nonetheless, other effects can also contribute to explain the presence of this phenomenon in porous media such as contact angle effects, entrapped air and pore network connectivity (e.g. Jury et al., 1991; Pham et al., 2005). Therefore, understanding of the pore geometry and the hydraulic properties at this scale is a key feature to describe and study the hydraulic properties at the macroscale.

Several analytical and numerical models have been proposed in the literature to study water flow at pore scale, the most widely used are the capillary tube models (e.g. Burdine, 1953; Mualem, 1976a), statistical distribution of pores (Or and Tuller, 1999; Xu and Torres-Verdín, 2013) and pore-network models (e.g. Bryant and Blunt, 1992; Blunt et al., 2002; Joekar-Niasar et al., 2010; Jougnot et al., 2019). In pore-network models, the pore space is represented by a grid of pores (i.e. larger void spaces) and throats (i.e. narrow openings that connect the pores) with parametrized geometries and topology which allow to numerically simulate the flow. The irregularity of the pore geometry is represented by different cross-sectional shapes as, for example, a star, a square or a triangle (e.g. Man and Jing, 1999; Blunt et al., 2002; Joekar-Niasar et al., 2010). Based on a gamma statistical distribution of pores, Tuller et al. (1999) and Or and Tuller (1999) developed a physically based model to calculate the hydraulic conductivity as a function of matric potential. At the pore scale, they assumed an angular pore space model composed of slit-shaped spaces connected to a wider unit cell. This cell represents angular pores with different cross-sectional shapes such as a triangle, a square or a circle. Nevertheless, on the basis of capillary tube models, a wide range of models have been developed since their simplicity to describe pore properties and to derive macroscale properties. In fact, the most widely used empirical and analytical models for predicting saturation and permeability curves assuming different pore size distributions have been derived assuming a capillary tube model (Brooks and Corey, 1964; Mualem, 1976b; Van Genuchten, 1980). In a recent study, Cai et al. (2022) reviewed the fundamentals and concepts of different imbibition models developed in the framework of capillary tube models over the past 100 years. Moreover, natural porous media show statistical behaviour similar to fractal scaling laws over multiple scales, thus fractal theory has been proven as an effective tool to describe the capillary size distribution of porous media. As a result, capillary models and fractal scaling laws can provide a valuable insight on the flow of porous media and, based on them, many researchers have derived expressions of the medium properties.

Petersen (1958) proposed a model to estimate the effective diffusivity under steady state conditions and studied the quantitative effect of periodic pore constrictions on that

72 property. To this aim, the author assumed the pore space represented by a bundle of capil-  
73 laries where each pore is modelled by a hyperbola of revolution giving a pore constriction  
74 at the vertex of the hyperbola. Guarracino et al. (2014) developed a physically-based  
75 model that describes saturated and relative permeability, porosity and retention curve of  
76 a porous medium by representing the pore space as cylindrical tortuous capillary tubes  
77 with periodic fluctuations in the radius of the pores and a fractal pore size distribution.  
78 The fluctuations considered by Guarracino et al. (2014) allowed them to include the hys-  
79 teresis phenomenon in the hydraulic properties. This model has recently been used by  
80 Rembert et al. (2020) to develop an analytical model to describe electrical conductivity  
81 in porous media. Wang et al. (2015) proposed an analytical model that estimates the  
82 permeability and average flow velocity in a porous medium as function of geometrical  
83 shape factors of capillaries, fractal dimensions and micro-structural parameters. In this  
84 model, the pore space is represented by a bundle of tubes with different geometrical shapes  
85 of their cross-sectional area. Soldi et al. (2017) developed a physically based analytical  
86 model to describe the hydraulic properties of a porous medium including the hysteresis  
87 phenomenon. To that end, the authors assumed a pore size distribution by following a  
88 fractal law and irregularities in the pore geometry. They introduced these irregularities  
89 in the model by considering each capillary as a cylindrical tube with periodic reductions  
90 of the capillary radius (i.e. consecutive segments of different constant radii). Recently,  
91 Stanić et al. (2020b) developed a physically based model of the water retention and hy-  
92 draulic conductivity of unsaturated soils which includes capillary and adsorption effects.  
93 The authors considered capillary-based water retention and hydraulic conductivity func-  
94 tions based on a multifractal grain size distribution, the Young-Laplace law and Mualem's  
95 model. Later and based on fractal geometry, Xu et al. (2020) derived a pore-scale model  
96 for fluid flow through porous media and studied the hydraulic tortuosity of the media.

97 In the framework of capillary tube models, we derive a new analytical constitutive  
98 model that considers a more realistic pore geometry for estimating hydraulic properties  
99 under partially saturated conditions. The pore space is represented by a bundle of cylin-  
100 drical capillaries whose radii follow a sinusoidal function with varying aperture along the  
101 pore length. In previous studies, the effect of changes in the geometry of the capillar-  
102 ies cross-sectional area has been examined for flow and medium properties (e.g. Or and  
103 Tuller, 1999; Wang et al., 2015). It is important to highlight that these studies analyzed  
104 different shapes of the capillaries but the aperture along each capillary tube is constant.  
105 In this study, we analyze the effects of pore geometry in hydraulic properties due to  
106 changes along the length of the capillaries (i.e. varying aperture). To this end, we com-  
107 pare the new model with the one proposed by Soldi et al. (2017) which assumes a bundle  
108 of cylindrical capillary tubes with straight periodic reductions in the pore radius. The  
109 geometry of the new model gives an advantage over that proposed by Soldi et al. (2017)  
110 due to the smooth variations of the pores radii which is a more realistic representation  
111 of a natural porous medium. Experimental descriptions of the pore geometry and fluid  
112 dynamics can be obtained due to the current developments in imaging technology which  
113 allow the direct microscopic measures by using X-ray tomography (e.g. Lindquist et al.,  
114 2000; Dong and Blunt, 2009) and high-speed cameras (e.g. Moebius and Or, 2012). It is

115 important to remark that the main difference between the geometries of the two studied  
116 models is in the longitudinal section and that the cross-section for both is circular. For  
117 the new model, we obtain analytical closed form expressions for the saturated and rel-  
118 ative hydraulic properties which depend on the geometrical parameters that define the  
119 pore structure, the tortuosity, the pore-size distribution and the radii of the pores. These  
120 expressions are then compared to the expressions of Soldi et al. (2017) model in order to  
121 analyze the effect of the different pore geometries in the hydraulic properties. To that  
122 aim, we perform a sensitivity analysis of these properties to changes in the geometrical  
123 parameters, and we test the estimates of the model against different sets of experimental  
124 data.

## 125 2 Constitutive models

126 In this section, we derive new closed-form analytical expressions for porosity, permeability,  
127 effective saturation and relative permeability in the framework of capillary tube models.  
128 First, we present the pore geometry of the model and develop some hydraulic properties  
129 which are valid for a single pore. Then, by upscaling the pore properties to a cylindrical  
130 representative elementary volume (REV) of a porous medium with a fractal pore size  
131 distribution, we obtain expressions for the hydraulic properties at the macroscale. This  
132 new model is compared with the model developed by Soldi et al. (2017). We also present  
133 in this section the pore geometry and the hydraulic properties obtained at the pore and  
134 the macroscopic scale from Soldi et al. (2017).

### 135 2.1 Pore geometry description

136 The constitutive model proposed by Soldi et al. (2017), from now on referred to as straight  
137 piecewise model, considers that, at the microscale, the pore structure of the medium is  
138 represented by capillary tubes with varying aperture. Each pore is conceptualized as a  
139 circular tube of radius  $R$  (m) and length  $l$  (m) with periodically straight pore throats of  
140 radius  $aR$  and length  $c\lambda$  (as shown in Fig.1). The factor  $a$  is defined as the radial factor  
141 which represents the ratio in which the radius of the pore is reduced. Assuming that the  
142 pore geometry has a wavelength  $\lambda$ , the factor  $c$  represents the fraction of  $\lambda$  with the pore  
143 throat. Then, the pore radius can be expressed for one wavelength as (Soldi et al., 2017):

$$r(x) = \begin{cases} R & \text{if } x \in [0, \lambda(1 - c)), \\ aR & \text{if } x \in [\lambda(1 - c), \lambda), \end{cases} \quad (1)$$

144 where the factors  $a$  and  $c$  vary between 0 and 1. Note that the model also considers that  
145 this geometry is replicated along a capillary tube and that the length of the tube contains  
146 an integer number  $M$  of wavelengths.

147 Under similar hypotheses and the previously defined  $a$  and  $c$  factors, a new pore  
148 geometry is considered for each capillary tube. While the cross-section of the pore is  
149 circular as in the previous geometry, the radius of each tube is variable in the constrictive

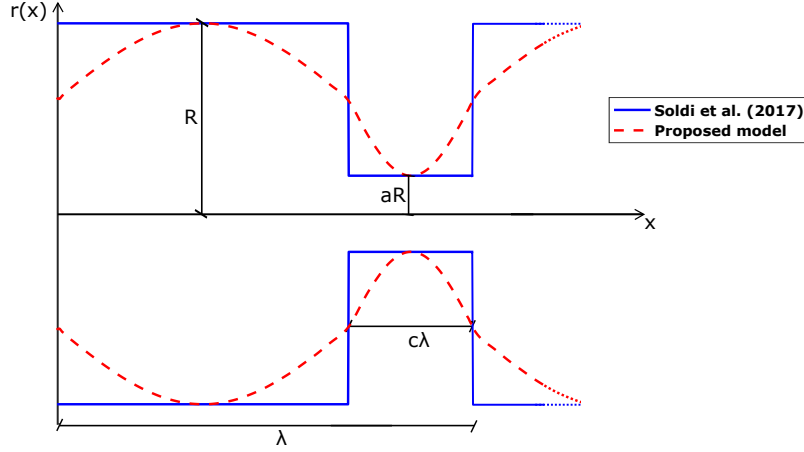


Figure 1: Pore geometry schemes for one wavelength of the constitutive models for a single capillary tube with periodic straight pore throats (blue) and periodic sinusoidal pore throats (red).

150 and also in the non-constrictive lengths of the pore (see Fig. 1). In this case, the pore  
 151 radius along one wavelength  $\lambda$  of the tube can be expressed as:

$$r(x) = \begin{cases} \frac{R}{2}(1+a) + \frac{R}{2}(1-a)\sin\left(\frac{\pi}{\lambda(1-c)}x\right) & \text{if } x \in [0, \lambda(1-c)), \\ \frac{R}{2}(1+a) + \frac{R}{2}(1-a)\sin\left(\frac{\pi}{\lambda c}[x - \lambda(1-2c)]\right) & \text{if } x \in [\lambda(1-c), \lambda). \end{cases} \quad (2)$$

152 Note that, for  $c = 0.5$ , Eq. (2) is equivalent to the model of Guarracino et al. (2014)  
 153 which considers the same length for the constrictive and non-constrictive fractions of the  
 154 sinusoidal pore geometry. Hereafter, we will refer to this proposed model as the sinusoidal  
 155 piecewise model.

156 Based on the above assumptions, expressions for the pore volume and volumetric water  
 157 flow in a single pore can be obtained. By integrating the cross-sectional area over the  
 158 length  $l$  of a capillary tube, the volume of a pore  $V_p$  ( $\text{m}^3$ ) can be calculated as follows:

$$V_p = \int_0^l \pi r^2(x) dx = \pi R^2 l f_v(a, c), \quad (3)$$

159 where the dimensionless factor  $f_v$  varies between 0 and 1, and quantifies the reduction in  
 160 the pore volume resulting from the presence of the pore throats. For the straight piecewise  
 161 model, the expression of this factor yields (Soldi et al., 2017)

$$f_v(a, c) = a^2 c + 1 - c, \quad (4)$$

162 while for the sinusoidal piecewise model,  $f_v$  is expressed as

$$f_v(a, c) = \frac{(1+a)^2}{4} + \frac{(1-a)^2}{8} + \frac{1}{\pi}(1-a^2)(1-2c). \quad (5)$$

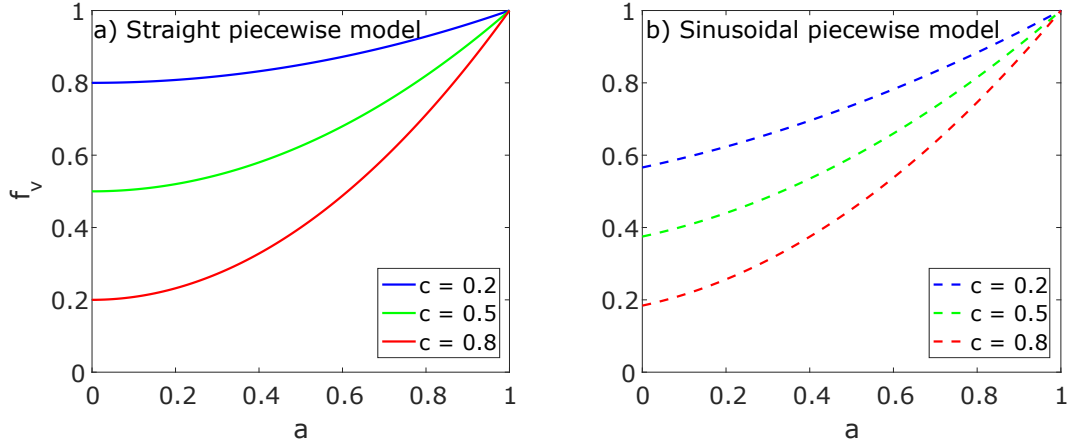


Figure 2: Dimensionless factor  $f_v$  as a function of the radial factor  $a$  for different constant values of parameter  $c$ : a)  $f_v$  factor of the straight piecewise model (Eq. (4)) and b)  $f_v$  factor of the sinusoidal piecewise model (Eq. (5)).

163 Note that for  $a = 1$ ,  $f_v = 1$  for both models and the expression obtained for Eq. (3)  
 164 represents the volume of a capillary tube of constant radius  $R$ . Figure 2 shows the  
 165 variation of  $f_v$  as a function of the radial factor  $a$  for different values of the length factor  
 166  $c$ . It can be observed that for a fixed value of  $a$ ,  $f_v$  of the straight piecewise model varies in  
 167 a wider range of values than the  $f_v$  factor of the sinusoidal piecewise model. Nevertheless,  
 168 for both models it can be noticed that the presence of the pore throats affects significantly  
 169 the volume of a pore.

170 Under the hypothesis of laminar flow and neglecting the convergence and divergence  
 171 of the flow, the volumetric water flow  $q_p$  ( $\text{m}^3 \text{s}^{-1}$ ) in the capillary tube represented by  
 172 the geometry of the straight piecewise model can be approximated with (Bodurtha, 2003;  
 173 Bousfield and Karles, 2004):

$$q_p = \frac{\rho g}{\mu} \left[ \frac{1}{l} \int_0^l \frac{8}{\pi r^4(x)} dx \right]^{-1} \frac{\Delta h}{l} = \frac{\rho g \pi}{\mu} \frac{R^4}{8} f_k(a, c) \frac{\Delta h}{l} \quad (6)$$

174 where  $\rho$  ( $\text{kg m}^{-3}$ ) is the water density,  $g$  ( $\text{m s}^{-2}$ ) gravity,  $\mu$  ( $\text{Pa s}$ ) water dynamic viscosity,  
 175  $\Delta h$  (m) the head drop across the tube and  $f_k$  a dimensionless factor given by (Soldi et al.,  
 176 2017)

$$f_k(a, c) = \frac{a^4}{c + a^4(1 - c)}. \quad (7)$$

177 This factor varies between 0 and 1, and quantifies the reduction in the volumetric flow  
 178 rate due to the pore throats.

179 Assuming the same flow conditions and following the work of Guarracino et al. (2014),  
 180 we calculate the volumetric flow for a capillary with sinusoidal piecewise geometry by  
 181 considering an average radius  $(R(1 + a)/2)$  and an equivalent permeability (Reis and

182 Acock, 1994):

$$q_p = \frac{\rho g}{\mu} \left[ \frac{1}{l} \int_0^l \frac{8}{\pi r^2(x)} dx \right]^{-1} \frac{R^2(1+a)^2}{4} \frac{\Delta h}{l} = \frac{\rho g \pi}{\mu} \frac{R^4}{8} f_k(a, c) \frac{\Delta h}{l}, \quad (8)$$

183 from this equation, the factor  $f_k$  for the sinusoidal piecewise model is found and computed  
184 as follows

$$f_k(a, c) = \left[ \frac{1}{l} \int_0^l \frac{dx}{r^2(x)} \right]^{-1} \frac{(1+a)^2}{4R^2}. \quad (9)$$

185 Substituting Eq. (2) in Eq. (9) and integrating, it yields

$$f_k(a, c) = \frac{a^{3/2}(1+a)}{2} \left\{ (1-2c) \left[ 1 - \frac{2}{\pi} \operatorname{tg}^{-1} \left( \frac{1-a}{2\sqrt{a}} \right) - \frac{4}{\pi} \frac{(1-a)\sqrt{a}}{(1+a)^2} \right] + 2c \right\}^{-1}. \quad (10)$$

186 The exact expression of  $f_k$  given by Eq. (10) can be reduced to the following approximate  
187 expression

$$f_k(a, c) = \frac{a^{3/2}\pi(1+a)^3}{2\pi(1+a)^2 - 4(1-a)(1-2c)(1+\sqrt{a})^2}. \quad (11)$$

188 It is interesting to observe that the final expressions of Eqs. (6) and (8) are similar except  
189 for the factor  $f_k$  which differs with the geometry of each model. The variation of  $f_k$  as a  
190 function of the radial factor  $a$  is shown in Fig. 3 for both models, for different values of  
191 the length factor  $c$ . Note that the factor  $f_k$  controls the volumetric water flow in a pore  
192 and varies significantly with the geometry. While for the straight piecewise model  $f_k$  (Eq.  
193 (7)) drastically reduce the volumetric flow of the pore for decreasing values of parameter  
194  $a$  (see Fig. 3a), for the sinusoidal piecewise model,  $f_k$  (Eq.(10)) produces gradual changes  
195 of the volumetric flow (Fig. 3b). Moreover, the  $f_k$  values for the sinusoidal piecewise  
196 model obtained by the exact and the approximate expressions (Eqs. (10) and (11)) are  
197 similar for all the range of parameter  $a$  values and for the different values of parameter  
198  $c$ . Note also that if  $a = 1$  then  $f_k = 1$ , and the expressions obtained for Eqs. (6) and (8)  
199 represent the volumetric flow of a capillary tube of constant radius  $R$ .

## 200 2.2 Hydraulic properties at REV scale

201 To derive the expressions of the hydraulic properties under total and partial saturation  
202 conditions, we consider a REV conceptualized as a circular cylinder of radius  $R_{REV}$  and  
203 length  $L$ . The pore structure of the REV is represented by a bundle of tortuous constrictive  
204 tubes with a fractal pore size distribution. We consider that the radius of the pores  
205  $R$  varies from a minimum value  $R_{min}$  to a maximum value  $R_{max}$  and that the tortuosity  
206  $\tau$  (dimensionless) defined as  $\tau = l/L$  is constant for all the bundle. Thus,  $\tau$  can be  
207 understood as an effective macroscopic value for all the pores of the REV.

208 Based on the fractal theory, the cumulative size distribution of pores is assumed to  
209 obey the following law (Tyler and Wheatcraft, 1990; Guarracino et al., 2014; Soldi et al.,  
210 2017; Rembert et al., 2020):

$$N(R) = \left( \frac{R_{REV}}{R} \right)^D \quad (12)$$

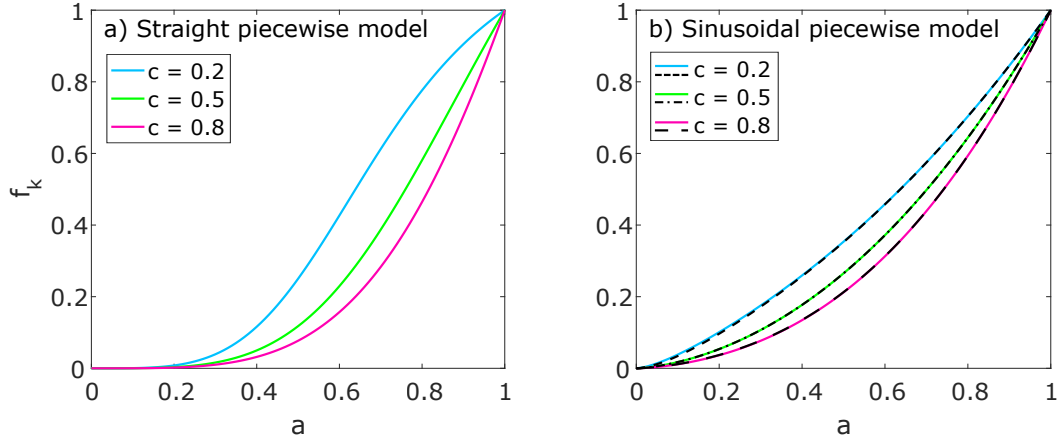


Figure 3: Dimensionless factor  $f_k$  as a function of the radial factor  $a$  for different constant values of parameter  $c$ : a)  $f_k$  factor of the straight piecewise model (Eq. (7)) and b)  $f_k$  factor of the sinusoidal piecewise model where the solid and dashed lines correspond to the exact and approximate expressions (Eqs. (10) and (11)), respectively.

211 where the radius of the pores remains in the range  $0 < R_{min} \leq R \leq R_{max} < R_{REV}$  and  $D$   
 212 (dimensionless) is the fractal dimension of the pores. By using the Sierpinski carpet which  
 213 is a classical fractal object, Tyler and Wheatcraft (1990) show that the fractal dimension  
 214  $D$  of Eq. (12) varies between 1 and 2 for different porous media. The number of pores  
 215 whose radii are within the infinitesimal range  $R$  and  $R + dR$  is obtained from Eq. (12)  
 216 as follows:

$$-dN(R) = DR_{REV}^D R^{-D-1} dR \quad (13)$$

217 where the minus sign implies that the number of pores decreases when the radius of the  
 218 pore increases (Yu et al., 2003; Thanh et al., 2019).

### 219 2.2.1 Porosity

220 The porosity of the REV  $\phi$  (dimensionless) can be obtained straightforward from its  
 221 definition as the quotient between the volume of pores and the volume of the REV as  
 222 follows:

$$\phi = \frac{\int_{R_{min}}^{R_{max}} V_p(R) dN(R)}{\pi R_{REV}^2 L}. \quad (14)$$

223 Then, replacing Eq. (3) in Eq. (14), it yields:

$$\phi = f_v(a, c) \frac{D\tau}{R_{REV}^{2-D}(2-D)} \left[ R_{max}^{2-D} - R_{min}^{2-D} \right] \quad (15)$$

224 being  $f_v$  the expression given by Eqs. (4) or (5) according to the geometry of the straight  
 225 and sinusoidal piecewise models, respectively. Note that for  $a = 1$ ,  $f_v = 1$  for both models  
 226 and the expression obtained for Eq. (15) represents the porosity of the REV considering

227 non-constrictive tortuous tubes. It can also be noticed that, if  $c = 0.5$ , Eqs. (5) and  
 228 (15) are consistent with the expressions of the model of Guarracino et al. (2014) when  
 229 considering the case of non-tortuous capillaries (i.e.  $\tau = 1$ ).

### 230 2.2.2 Permeability

231 We first calculate the volumetric flow rate  $q$  ( $\text{m}^3 \text{s}^{-1}$ ) at REV scale in order to obtain  
 232 the permeability of the REV. On the one hand, similar to the approach used by Yu et al.  
 233 (2002, 2003), Soldi et al. (2017) and Chen et al. (2021), the flow  $q$  can be calculated by  
 234 integrating all the pores volumetric flow rates given by Eq. (6) or (8) over the entire range  
 235 of pore sizes:

$$q = \int_{R_{min}}^{R_{max}} q_p(R) dN(R) = \frac{\rho g \pi}{\mu} \frac{DR_{REV}^D}{8(4-D)} f_k \frac{\Delta h}{l} [R_{max}^{4-D} - R_{min}^{4-D}]. \quad (16)$$

236 On the other hand, the volumetric flow through the REV can be expressed by Darcy's  
 237 law for saturated porous media (Darcy, 1856) as:

$$q = \frac{\rho g}{\mu} k \pi R_{REV}^2 \frac{\Delta h}{L} \quad (17)$$

238 where  $k$  ( $\text{m}^2$ ) is the permeability of the REV. Then, combining Eqs. (16) and (17) yields:

$$k = f_k(a, c) \frac{DR_{REV}^{D-2}}{8\tau(4-D)} [R_{max}^{4-D} - R_{min}^{4-D}] \quad (18)$$

239 where  $f_k$  is the expression given by Eq. (7) or (10) for the straight and sinusoidal piecewise  
 240 models, respectively. Note that in the case of non-constrictive tubes (i.e.,  $a = 1$ ),  $f_k = 1$   
 241 for both models and Eq. (18) describes the permeability of the REV with straight tortuous  
 242 tubes. Also, note that if we consider non-tortuous capillaries,  $\tau = 1$ , and  $c = 0.5$ , Eqs.  
 243 (10) and (18) are consistent with the expressions of the sinusoidal model of Guarracino  
 244 et al. (2014).

### 245 2.2.3 Retention and Relative Permeability Curves

246 It is well-known that retention and relative permeability curves obtained from drainage  
 247 and imbibition tests are different due to the hysteresis phenomenon. The effect of this  
 248 phenomenon on those curves can be easily modeled with the pore geometries illustrated  
 249 in Fig. 1 and described by Eqs. (1) and (2). We derive those curves expressions for  
 250 the sinusoidal piecewise model similar to the approach used by Soldi et al. (2017) for the  
 251 straight piecewise model and also by Guarracino et al. (2014) and by Chen et al. (2021).

252 The main drying effective saturation curve is obtained by considering that the REV  
 253 is initially fully saturated and is drained by a pressure head  $h$  (m). This pressure can be  
 254 related to a pore radius  $R_h$  by the following equation (Bear, 1998):

$$h = \frac{2T_s \cos(\beta)}{\rho g R_h}, \quad (19)$$

255 where  $T_s$  ( $\text{N m}^{-1}$ ) is the surface tension of the water and  $\beta$  the contact angle. Note  
 256 that Eq. (19) is the Young-Laplace equation which is valid for straight tubes. However,  
 257 this equation can be used for the geometry described by Eq. (2) when considering that  
 258 the pressure head value changes with the position of the wetting perimeter (Guarracino  
 259 et al., 2014). The pore radius that corresponds to this position is the radius of the pore  
 260 throat for both geometries,  $R_h = aR$ . Therefore, we assume that a tube becomes fully  
 261 desaturated if its pore throat radius is greater than the radius  $R_h$  given by Eq. (19). It is  
 262 then reasonable to also assume that pores within the range  $R_{min} \leq R \leq R_h/a$  will remain  
 263 fully saturated, and the main drying effective saturation curve  $S_e^d$  (dimensionless) can be  
 264 expressed by:

$$S_e^d = \frac{\int_{R_{min}}^{R_h/a} V_p(R) dN(R)}{\int_{R_{min}}^{R_{max}} V_p(R) dN(R)} = \frac{(R_h/a)^{2-D} - R_{min}^{2-D}}{R_{max}^{2-D} - R_{min}^{2-D}}. \quad (20)$$

265 The  $S_e^d$  curve can also be expressed as a function of the pressure head by substituting Eq.  
 266 (19) in (20):

$$S_e^d(h) = \begin{cases} 1 & \text{if } h \leq \frac{h_{min}}{a} \\ \frac{(ha)^{D-2} - h_{max}^{D-2}}{h_{min}^{D-2} - h_{max}^{D-2}} & \text{if } \frac{h_{min}}{a} < h < \frac{h_{max}}{a} \\ 0 & \text{if } h \geq \frac{h_{max}}{a}, \end{cases} \quad (21)$$

267 where

$$h_{min} = \frac{2T_s \cos(\beta)}{\rho g R_{max}} \quad \text{and} \quad h_{max} = \frac{2T_s \cos(\beta)}{\rho g R_{min}}, \quad (22)$$

268  $h_{min}$  and  $h_{max}$  are the minimum and maximum pressure heads defined by  $R_{max}$  and  $R_{min}$ ,  
 269 respectively.

270 Similarly, for an imbibition experiment, the main wetting effective saturation curve  
 271  $S_e^w$  (dimensionless) can be obtained assuming that the REV is initially dry and it is  
 272 flooded with a pressure  $h$ . Only the tubes whose radius  $R$  is smaller than  $R_h$  will be fully  
 273 saturated in this case and the  $S_e^w$  curve can be computed as:

$$S_e^w(h) = \begin{cases} 1 & \text{if } h \leq h_{min} \\ \frac{h^{D-2} - h_{max}^{D-2}}{h_{min}^{D-2} - h_{max}^{D-2}} & \text{if } h_{min} < h < h_{max} \\ 0 & \text{if } h \geq h_{max}. \end{cases} \quad (23)$$

274 To obtain the relative permeability curves, we consider the same hypotheses and ne-  
 275 glect film flow on surfaces of the tubes. During a drainage experiment, the pores that  
 276 contribute to the total volumetric flow through the REV  $q$  ( $\text{m}^3\text{s}^{-1}$ ) are those that remain  
 277 saturated ( $R_{min} \leq R \leq R_h/a$ ). Then,  $q$  can be obtained by integrating the individual  
 278 volumetric flow rates  $q_p$  given by Eq. (6) or (8) as follows (similar to Yu et al. (2002) and  
 279 Yu (2008)):

$$q = \int_{R_{min}}^{R_h/a} q_p(R) dN(R). \quad (24)$$

280 Based on Buckingham-Darcy law for unsaturated water flow (Buckingham, 1907), the  
 281 volumetric flow through the REV can be expressed by:

$$q = \frac{\rho g}{\mu} k k_{rel} \pi R_{REV}^2 \frac{\Delta h}{L} \quad (25)$$

282 where  $k_{rel}$  (dimensionless) is the relative permeability. Combining Eqs. (24) and (25), an  
 283 expression for the main drying relative permeability curve  $k_{rel}^d$  can be obtained:

$$k_{rel}^d(R_h) = \frac{(R_h/a)^{4-D} - R_{min}^{4-D}}{R_{max}^{4-D} - R_{min}^{4-D}}. \quad (26)$$

284 Using Eq. (19) we can express Eq. (26) as a function of the pressure head:

$$k_{rel}^d(h) = \begin{cases} 1 & \text{if } h \leq \frac{h_{min}}{a} \\ \frac{(ha)^{D-4} - h_{max}^{D-4}}{h_{min}^{D-4} - h_{max}^{D-4}} & \text{if } \frac{h_{min}}{a} < h < \frac{h_{max}}{a} \\ 0 & \text{if } h \geq \frac{h_{max}}{a}. \end{cases} \quad (27)$$

285 Otherwise, for an imbibition experiment, the main wetting relative permeability curve  
 286  $k_{rel}^w$  can be derived similarly by integrating Eq. (24) over the range of saturated pores  
 287 ( $R_{min} \leq R \leq R_h$ ):

$$k_{rel}^w(h) = \begin{cases} 1 & \text{if } h \leq h_{min} \\ \frac{h^{D-4} - h_{max}^{D-4}}{h_{min}^{D-4} - h_{max}^{D-4}} & \text{if } h_{min} < h < h_{max} \\ 0 & \text{if } h \geq h_{max}. \end{cases} \quad (28)$$

288 Note that Eqs. (21), (23), (27) and (28) can be used to calculate the main drying and  
 289 wetting curves of the hysteretic cycle observed in the effective saturation and relative  
 290 permeability. These expressions have analytical closed forms with only four independent  
 291 parameters with geometrical or physical meaning ( $a$ ,  $D$ ,  $h_{min}$  and  $h_{max}$ ). It can also be  
 292 noted that these relative properties of the medium ( $S_e$  and  $k_{rel}$ ) have the same expressions  
 293 for both the sinusoidal and straight piecewise models and are independent of the length  
 294 factor  $c$  of the geometries. Therefore, variations of the pore geometry affect only the  
 295 expressions of the porosity  $\phi$  and permeability  $k$  of the medium while no effects are  
 296 present in the relative hydraulic properties.

#### 297 **2.2.4 Relationships between the hydraulic properties**

298 In this section, we derive relationships between the macroscopic hydraulic properties  
 299 of the porous medium, porosity and permeability, and effective saturation and relative  
 300 permeability following the approach used by Soldi et al. (2017).

301 In order to obtain a relationship between permeability  $k$  and porosity  $\phi$ , we assume  
 302 that  $R_{min} \ll R_{max}$  and then the terms  $R_{min}^{2-D}$  and  $R_{min}^{4-D}$  can be considered negligible in  
 303 Eqs. (15) and (18). Indeed, for most porous media, the ratio between the  $R_{min}$  and  $R_{max}$   
 304 values is smaller than  $10^{-2}$  (e.g. Yu and Li, 2001). Under this assumption and combining  
 305 the resulting expressions, we obtain the following equation:

$$k(\phi) = \frac{DR_{REV}^2}{8\tau(4-D)} f_k(a, c) \left( \frac{2-D}{D\tau f_v(a, c)} \right)^{\frac{4-D}{2-D}} \phi^{\frac{4-D}{2-D}}. \quad (29)$$

306 This equation allows to estimate the permeability as function of porosity while also de-  
 307 pending on the pore geometry factors ( $a$  and  $c$ ) through the factors  $f_v$  and  $f_k$ , the fractal  
 308 dimension, the tortuosity and the radius of the REV. Given the similarity of the  $k$  and  
 309  $\phi$  expressions of the sinusoidal and straight piecewise models, the  $k(\phi)$  relationship can  
 310 be used for both models by taking into account the respective  $f_v$  and  $f_k$  factors of each  
 311 model. Note that, in the limit case of  $D = 1$ , Eq. (29) becomes similar to the Kozeny-  
 312 Carman equation (Kozeny, 1927; Carman, 1937). The relative permeability  $k_{rel}$  and  
 313 effective saturation  $S_e$  are estimated as function of a pore radius  $R_h$  by Eqs. (20) and  
 314 (26). Nevertheless, these equations can be combined to obtain a relationship between  $k_{rel}$   
 315 and  $S_e$  for both the drying and imbibition experiments and yields:

$$k_{rel}(S_e) = \frac{[S_e (\alpha^{D-2} - 1) + 1]^{\frac{4-D}{2-D}} - 1}{\alpha^{D-4} - 1} \quad (30)$$

316 where  $\alpha = R_{min}/R_{max}$ . Note that Eq. (30) has the same expression for both the straight  
 317 and sinusoidal piecewise models. It is also interesting to remark that, when  $k_{rel}$  is ex-  
 318 pressed in terms of  $S_e$ , the function obtained is non-hysteretic. This means that the  
 319 relationship between these two relative hydraulic properties is unique for the drying and  
 320 imbibition which is in agreement with a number of experimental data (e.g. Topp and  
 321 Miller, 1966; Van Genuchten, 1980; Mualem, 1986).

322  
 323 The model presented in this section is derived in the framework of capillary tube  
 324 models. There are two characteristic limitations that affect the models based on this  
 325 framework (e.g. Chen et al. 2021). The first limitation is that the lateral connectivity  
 326 in between the pores is not considered in the capillary system. There are no points of  
 327 intersection between capillaries and all of them run parallel with the same orientation.  
 328 The second limitation is that the hysteresis phenomenon on hydraulic properties cannot  
 329 be described by classical capillary tube models since the assumption of capillaries with  
 330 constant aperture is a very strong idealization for a real pore channel. Nevertheless,  
 331 the proposed model assumes irregularities in the pores which allows us to include this  
 332 phenomenon in effective saturation and relative permeability.

### 3 Sensitivity analysis of the geometrical parameters

In this section, a sensitivity analysis of the geometrical parameters of the models is addressed to study the effect of the pore structure on the hydraulic properties. Hence, we perform a parametric analysis of Eqs. (15) and (18) to estimate the porosity and permeability of the REV using Eqs. (4) and (7), and (5) and (10) to calculate the  $f_v$  and  $f_k$  factors for the straight and sinusoidal piecewise models, respectively. We test the influence of the radial factor  $a$  that controls the pore throats amplitude and the length factor  $c$  which controls the pore throats length. The estimates of  $\phi$  and  $k$  also depend on other characteristics of the porous medium, for both models, the following values are then considered:  $R_{REV} = 5$  cm,  $D = 1.5$ ,  $\tau = 1.4$ ,  $R_{min} = 1.5 \times 10^{-4}$  mm and  $R_{max} = 1.5$  mm.

Figure 4 summarizes this analysis and shows how the pore geometry modifies the macroscopic values of the properties. For low values of parameter  $c$ , the porosity estimated by the straight piecewise model is higher than the corresponding to the sinusoidal piecewise model (see Fig. 4a and 4b). This difference in the porosity is schematically represented by the grey area in Figure 4c-e where the pore geometry is shown for different values of parameters  $a$  and  $c$ . It can be seen that the area of the constrictive fraction of the pore is greater for the sinusoidal piecewise model than for the straight piecewise model. However, this excess area is smaller than the excess area of the straight piecewise model in the non-constrictive fraction of the pore. In these cases, the effect of geometry on porosity causes changes in this property of 5-10% approximately between the models. Figure 4f-g show the estimates of permeability which present different patterns of variation for the models. Note that for high values of parameter  $c$ , the permeability estimates of the straight piecewise model decrease faster than the estimates of the sinusoidal piecewise model when decreasing parameter  $a$ . However, the greatest differences between the permeability estimates are associated to low values of parameter  $c$  (short pore throats) over the entire range of parameter  $a$ . It can also be noticed that both models can estimate media with high permeability and high porosity, and also with low permeability and high porosity. Therefore, these models are able to represent a wide range of porous media. Although the straight piecewise model might consider a more simple pore shape structure, the sinusoidal piecewise model's geometry has the advantage of being more similar to a real porous media since it presents no abrupt changes between the constrictive and non-constrictive fractions of the pore.

The hysteresis phenomenon caused by the irregularities in the pore structure is explicitly observed in the effective saturation ( $S_e$ ) and relative permeability ( $k_{rel}$ ) when expressed as functions of the pressure head (Eqs. (21), (23), (27) and (28)). It is important to remark that the main drying and wetting curves of  $S_e$  and  $k_{rel}$  obtained for the straight and sinusoidal piecewise models have the same analytical expressions. Therefore, under the hypotheses of these models, considering the pore shape as straight or sinusoidal piecewise has no influence on  $S_e$  and  $k_{rel}$ . However, the expressions of  $S_e$  and  $k_{rel}$  depend on the geometrical parameter  $a$  while they are independent of parameter  $c$ . For this reason, we only test the effect of  $a$  that controls the amplitude of the pore throats

375 geometry. We consider the same reference values used for the previous sensitivity analysis  
376 for parameters  $D$ ,  $R_{min}$  and  $R_{max}$ . Figure 5 shows the effect of the radial factor  $a$  in the  
377 curves of the hydraulic properties  $S_e$  and  $k_{rel}$ . It can be observed that the influence of  
378 this parameter is significant in the main drying curves of  $S_e$  and  $k_{rel}$  for the entire range  
379 of pressure head values. Nevertheless, no effect of this parameter is observed on the main  
380 wetting curves of both properties since Eqs. (23) and (28) are independent of  $a$ . Note that  
381 the hysteresis cycle for  $S_e$  and  $k_{rel}$  increases for low values of  $a$  since the limit pressure  
382 head values ( $h_{min}/a$  and  $h_{max}/a$ ) of the main drying curves (Eqs. (21) and (27)) shift to  
383 higher values, which increases the distance between the main drying and wetting curves.  
384 Nonetheless, the two main curves of  $S_e$  and  $k_{rel}$  tend to reduce their distance when  $a$   
385 tends toward 1, as it can be expected since this limit case represents a tube of constant  
386 radius and thus no hysteretic phenomenon is observed in straight capillaries.

387 From this parametric analysis, we can conclude that the presence of constrictivities  
388 defined by parameters  $a$  and  $c$  leads to differences in the estimates of  $\phi$  and  $k$ , while only  
389 parameter  $a$  affects the estimates of  $S_e$  and  $k_{rel}$ . The most significant variations on the  
390  $\phi$  and  $k$  estimates are reached for low values of parameter  $c$ . Furthermore, an interesting  
391 result is that both models allows to represent porous media with high porosity and low  
392 permeability such as clays which cannot be properly represented with straight capillary  
393 models. The analysis of the relative hydraulic properties shows that the estimates of the  
394 main drying  $S_e$  and  $k_{rel}$  curves are highly sensitive to parameter  $a$  and that the greatest  
395 differences between the the main drying and wetting  $S_e$  and  $k_{rel}$  curves are observed for  
396 decreasing values of  $a$ .

## 397 4 Comparison with experimental data

398 In the present section, we test the ability of the proposed model to reproduce available  
399 measured data from the research literature. These data sets consist of measured perme-  
400 ability–porosity, hydraulic conductivity–pressure head, water content–pressure head and  
401 hysteretic water content–pressure values for different soil textures.

### 402 4.1 Water content and hydraulic conductivity laboratory data

403 In order to test the estimates of the proposed model, we selected three experimental data  
404 sets from different soil textures: a coarse granular material named GW Substrate from  
405 Stanić et al. (2020a), a well graded sand and a silty clay sand named Okcheon 2 and  
406 Seochang, respectively, from Oh et al. (2015). These data series consist of water content  
407 and hydraulic conductivity values as a function of pressure head which were measured  
408 during drainage experiments. As it is well known, hydraulic conductivity  $K$  (mD) and  
409 permeability  $k$  are related through  $K = k\rho g/\mu$ , while water content  $\theta$  (dimensionless) is  
410 related to saturation  $S$  through the porosity  $\phi$  of the medium. The test of the sinusoidal  
411 piecewise model relies on fitting Eqs. (15) and (21), and Eqs. (18) and (27) for the water  
412 content and the hydraulic conductivity data sets, respectively.

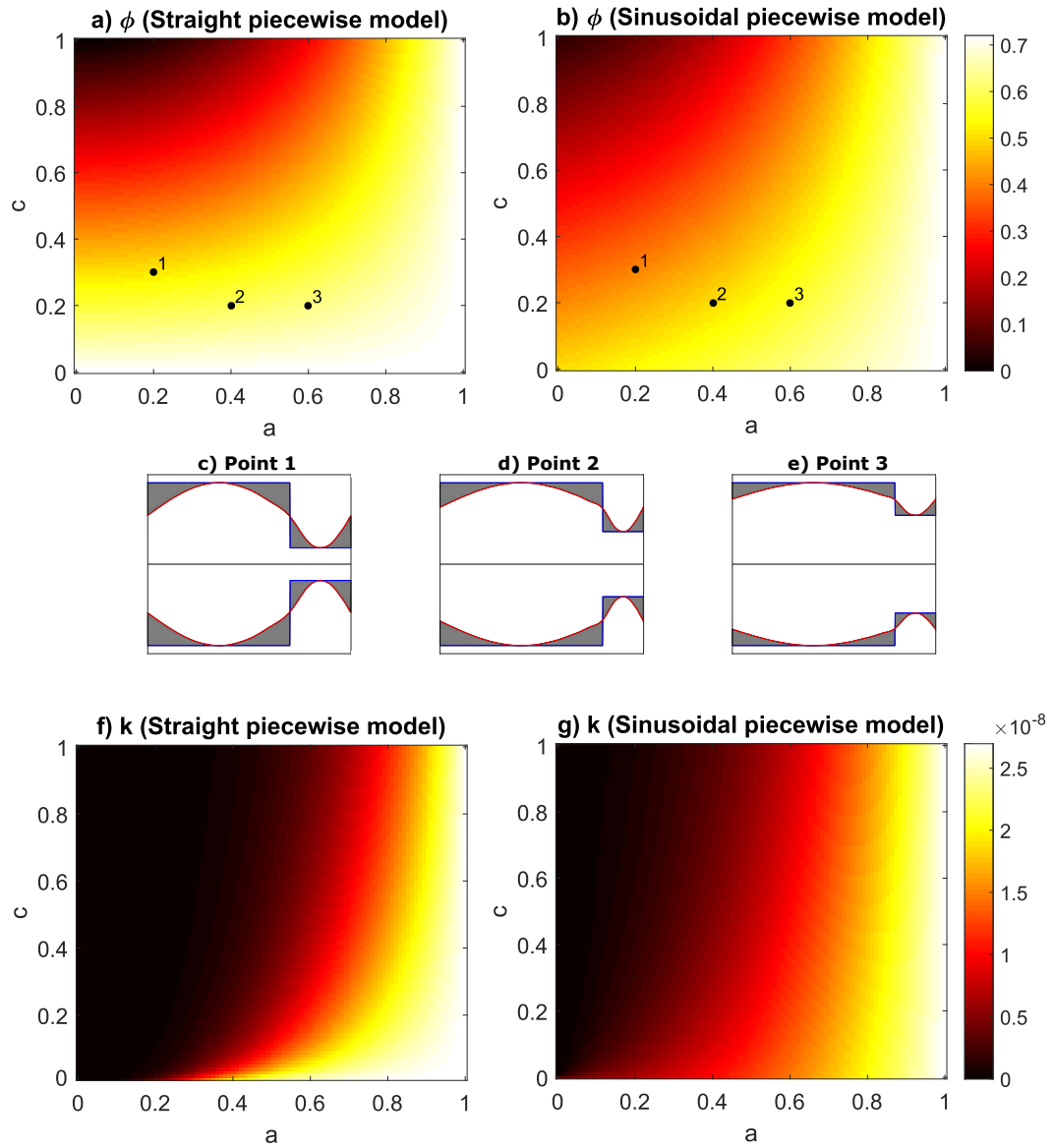


Figure 4: Parametric analysis of the porosity and permeability as functions of the radial and length factors,  $a$  and  $c$ , respectively: a) and f) for the straight piecewise model (Soldi et al., 2017), b) and g) for the sinusoidal piecewise model. Note that fixed values of the remaining parameters were considered in each case. Figs. c, d and e) show schematic representations of the pore structure for  $a = 0.2$  and  $c = 0.3$ ,  $a = 0.4$  and  $c = 0.2$ , and  $a = 0.6$  and  $c = 0.2$ , respectively, for the straight and sinusoidal piecewise models. The grey area indicates the difference in the pore volume between the models.

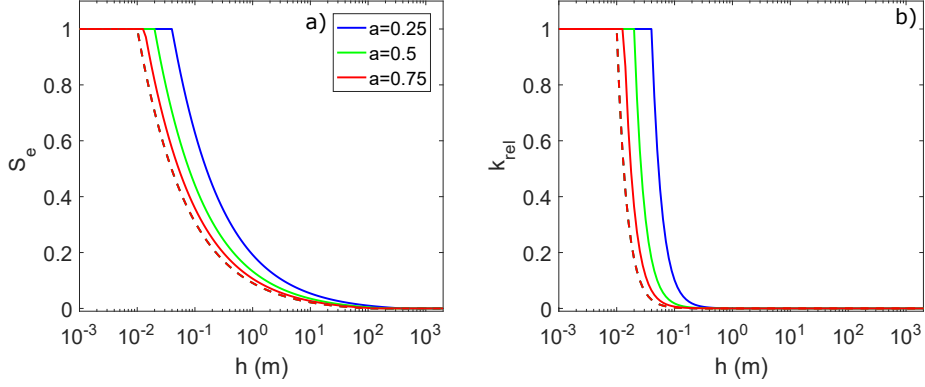


Figure 5: Parametric analysis of the relative properties: a) effective saturation and b) relative permeability, for drainage (solid lines) and imbibition (dashed lines), sensitivity to the radial factor  $a$ . In each case, fixed values of the remaining parameters are considered.

Table 1: Values of the fitted parameters ( $D$ ,  $\tau$ ,  $a$  and  $c$ ) for the water content and hydraulic conductivity curves using the sinusoidal piecewise model, and the corresponding values of  $h_{min}$  and  $h_{max}$ .

Soil type	Sinusoidal piecewise model parameters					
	$D$	$\tau$	$a$	$c$	$h_{min}$ (m)	$h_{max}$ (m)
Okcheon 2	1.729	1.257	0.35	0.78	0.297	$5 \times 10^4$
Seochang	1.711	1.296	0.41	0.85	0.367	$10 \times 10^3$
GW substrate	1.601	1.198	0.58	0.70	0.154	$50 \times 10^4$

413 Figure 6 illustrates the fit between the sinusoidal piecewise model and the experimental  
414 data sets. Table 1 lists the fitted parameters ( $D$ ,  $\tau$ ,  $a$  and  $c$ ). These parameters have  
415 been estimated by an exhaustive search method by minimizing the weighted normalized  
416 error between calculated and experimental data values for both the water content and  
417 hydraulic conductivity curves simultaneously. This model also requires specifying the  
418 minimum and maximum pressure heads which are determined by trial-and-error method,  
419 as well as the REV radius that is taken from Stanić et al. (2020a) and Oh et al. (2015) in  
420 order to reduce the number of the fitting parameters. Note that the sinusoidal piecewise  
421 model fits fairly well the data and can estimate the order of magnitude of the hydraulic  
422 properties for the different soils. It is interesting to remark that the model is able to  
423 reproduce the behaviour of the data with only one set of parameters for both hydraulic  
424 properties simultaneously.

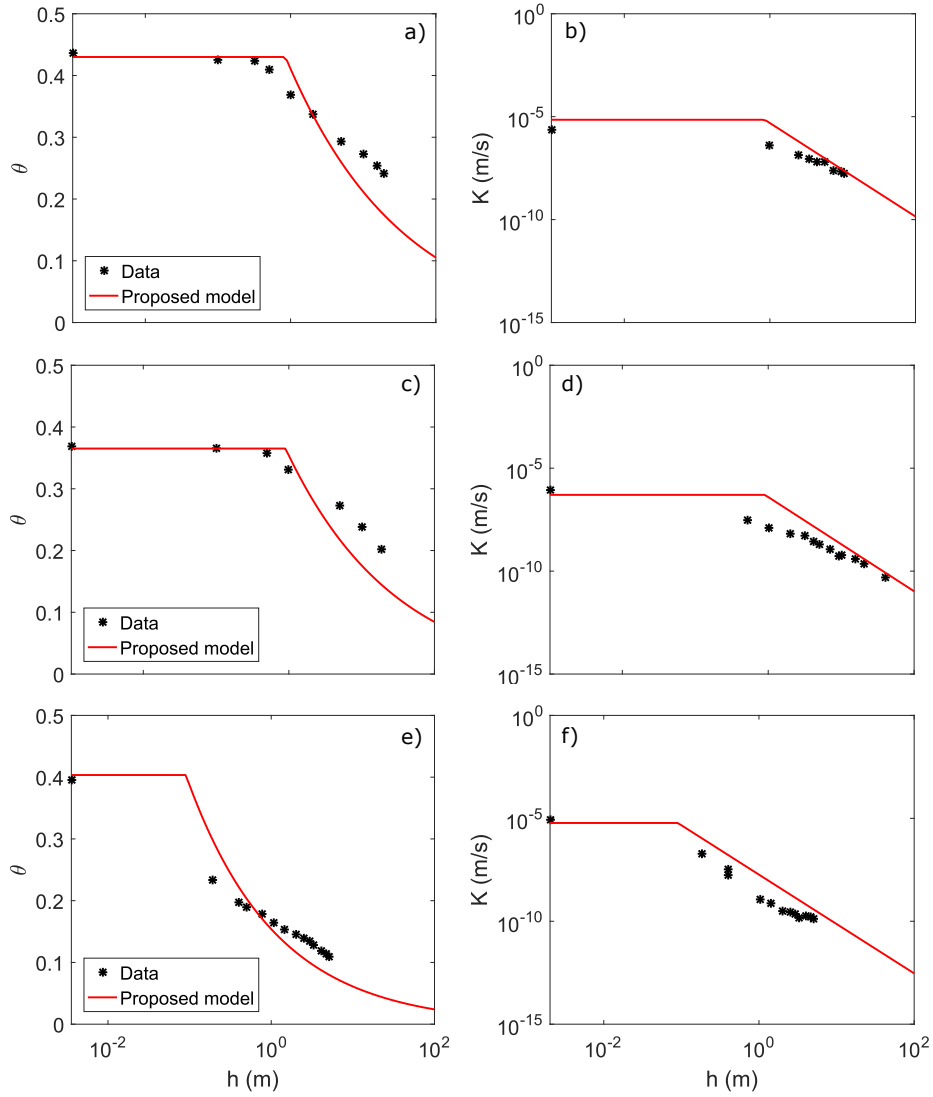


Figure 6: Comparison of the water content and hydraulic conductivity curves from the sinusoidal piecewise model with experimental data sets for a drainage experiment: a-b) okcheon 2, c-d) seochang (data from Oh et al., 2015) and e-f) GW substrate (data from Stanić et al., 2020a).

## 4.2 Permeability-porosity relationship

In Section 2.2.4 we derived a relationship between permeability and porosity (Eq. (29)) that depends on the geometry of the model through the factors  $f_v(a, c)$  and  $f_k(a, c)$ . We selected experimental data series from two different types of clays (an illite and a kaolinite) from Mesri and Olson (1971) to test the estimates of this equation. These estimates are calculated for both the sinusoidal and straight piecewise models using their respective relationship with the factors  $f_v$  and  $f_k$  of each model (Eqs. (5) and (10), and (4) and (7), respectively). In addition, we compare these relationships with the most classical equation to represent permeability-porosity data, the Kozeny-Carman equation (Kozeny, 1927; Carman, 1937), that can be expressed as follows:

$$k = \alpha_{KC} \frac{\phi^3}{(1 - \phi)^2} \quad (31)$$

being  $\alpha_{KC}$  a parameter that depends on the specific internal surface area, the tortuosity and an empirical geometrical parameter.

The model parameters have been estimated using an exhaustive search method, which is a simple and very robust technique. To apply this method, we use the admissible ranges for each parameter:  $0 < a, c < 1$  and  $1 < D < 2$ , and we consider  $1 < \tau < 2$  as representative values of tortuosity in a sedimentary porous medium. The exhaustive search method computes the error between data and predicted values for all possible combinations of the model parameters values and selects the ones that minimize the root-mean-square deviation (RMSD) between the calculated and experimentally measured values. Figure 7 shows the fits of the proposed relationships for both piecewise models (Eq. (29)) and the Kozeny-Carman equation (Eq. (31)). Table 2 lists the fitted parameters for the equations as well as their respective RMSD. Note that for Eq. (29), we fit parameters  $D$ ,  $\tau$ ,  $a$  and  $c$  for the sinusoidal and straight piecewise models. Eq. (29) also requires a  $R_{REV}$  value for which we consider the value from Mesri and Olson (1971),  $R_{REV} = 5$  cm. It is important to remark that the values of parameters  $D$  and  $\tau$  are the same for both models since they describe the same soil. Hence, we are able to highlight the effects of geometry through the fitting of the radial  $a$  and length  $c$  factors of each model. It can be observed that the proposed relationships fit fairly well both data sets for the entire range of porosities (Fig. 7). The geometry of the pores given by the fitted parameters presents smooth variations between the constrictive and non-constrictive fractions since the high values of  $c$  and  $a$  represent that the length of the pore throat is large and that the pore throat radius varies slightly from the pore radius. The comparison with the Kozeny-Carman equation shows that the proposed relationships provide much more better estimates. Indeed, it can be noted that the difference between the RMSD of the sinusoidal and straight piecewise models is not significant, and that they are smaller than the ones obtained from the fit of the Kozeny-Carman equation for both data sets.

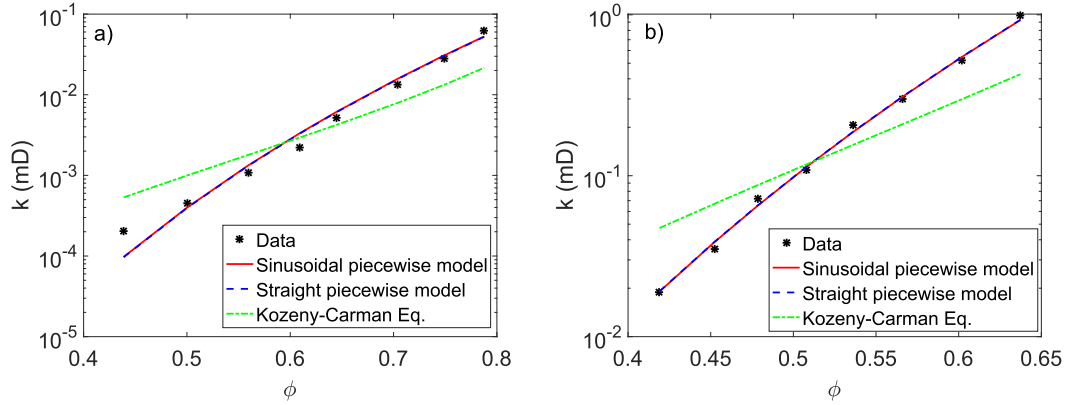


Figure 7: Comparison among the estimates of Eq. (29) for the sinusoidal and straight piecewise models, the Kozeny-Carman equation and experimental data sets of permeability-porosity for: a) illite and b) kaolinite (data from Mesri and Olson (1971)).

Table 2: Values of the fitted parameters ( $D$ ,  $\tau$ ,  $a$  and  $c$ ) and the RMSD for Eq. (29) when considering the sinusoidal and straight piecewise models, and for the Kozeny-Carman equation (Eq. (31)).

Model parameters	Soil type	
	Illite	Kaolinite
Sinusoidal piecewise model		
$D$	1.795	1.758
$\tau$	1.46	1.60
$a$	0.92	0.90
$c$	0.91	0.79
RMSD	0.1421	0.0301
Straight piecewise model (Soldi et al., 2017)		
$D$	1.795	1.758
$\tau$	1.46	1.60
$a$	0.90	0.89
$c$	0.60	0.70
RMSD	0.1422	0.0303
Kozeny-Carman (Eq. (31))		
$\alpha_{KC}$	0.002	0.217
RMSD	0.3032	0.2447

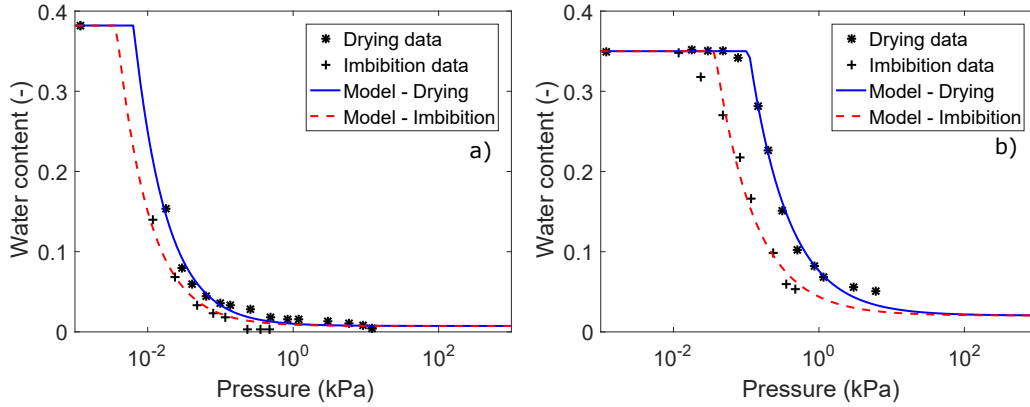


Figure 8: Comparison of the main drying and wetting water content curves with experimental data sets: a) gravelly sand and b) medium sand (data from Yang et al. (2004)).

### 461 4.3 Hysteresis in the water content

462 The performance of the model to describe the hysteresis phenomenon on the relative hy-  
 463 draulic property is tested by using available data from the literature. These experimental  
 464 data consist of two sets of measured water content and pressure values for two different  
 465 sands from Yang et al. (2004). Eqs. (21) and (23) are used to estimate the main drying  
 466 and wetting effective saturation curves which are then converted to water content values  
 467 in order to compare with the data.

468 Figure 8 shows the main drying and wetting water content curves fitted with the  
 469 proposed model for the two sands. The best-fitted parameters ( $D$ ,  $a$ ,  $h_{min}$  and  $h_{max}$ ) are  
 470 listed in Table 3 as well as the RMSD values for each sand. Note that the hysteretic  
 471 behavior of the water content can be satisfactorily reproduced by the model (see Fig. 8).  
 472 It can also be observed that for the gravelly sand the distance between the main drying  
 473 and wetting curves is smaller than for the main curves of the medium sand. This result  
 474 can be related to the size distribution and geometry of the pores which are represented  
 475 in the model by the fractal dimension  $D$  and the radial factor  $a$ . Comparing the values  
 476 of  $D$  and  $a$  shown in Table 3, note that the lowest value of  $D$  is obtained for the gravelly  
 477 sand which can be expected since low fractal dimensions values are associated to coarse  
 478 textured soils and the high values of the radial factor  $a$  represent less constrictive pores.  
 479 In fact, higher values of  $a$  represent pores with greater volume and thus a soil with higher  
 480 porosity. From the measured porosity values by Yang et al. (2004), it can be noted  
 481 that these geometrical results from the estimates of the models are consistent with the  
 482 experimental measures that evidence the higher porosity of the gravelly sand (38.2%) over  
 483 the medium sand (35%).

Table 3: Values of the fitted parameters ( $D$ ,  $a$ ,  $h_{min}$  and  $h_{max}$ ) for the water content main drying and wetting curves, and the corresponding RMSD.

Soil type	Models parameters				
	$D$	$a$	$h_{min}$ (kPa)	$h_{max}$ (kPa)	RMSD
Medium sand	1.19	0.34	0.037	910	0.0264
Gravelly sand	1.03	0.58	0.004	70	0.0126

## 5 Discussion and Conclusions

The present study is focused on the analysis of pore geometry effects in the hydraulic properties of porous media. We compare two constitutive analytical models based on physical and geometrical concepts which include the hysteresis phenomenon in the hydraulic properties by considering irregularities in the structure of the pores. The straight piecewise model (Soldi et al., 2017) assumes that the pore space is represented by a bundle of tortuous capillary tubes with straight periodic reductions in the pore radius, while the sinusoidal piecewise model developed in this study represents the pore space as a bundle of sinusoidal tortuous capillaries with varying aperture. Based on a fractal distribution of pore sizes and upscaling procedures at pore and REV scales, analytical closed-form expressions are obtained for porosity, permeability, effective saturation and relative permeability. These expressions depend on independent parameters:  $a$ ,  $c$ ,  $D$ ,  $\tau$ ,  $R_{min}$ ,  $R_{max}$  and  $R_{REV}$ , all of them with a specific physical or geometrical meaning.

Capillary tube models have been proposed for over 100 years and have provided a valuable insight into the characterization of flow and hydraulic properties of porous media (Cai et al., 2022). Some of the most well-known models based on this approach of capillary tubes are the van Genuchten and the Brooks and Corey models. However, since these models assume cylindrical tubes of constant radii, they cannot describe the hysteresis phenomenon present in the hydraulic properties. The hysteresis has been easily included in the proposed model due to its pore geometry with variable radius, enhancing the hypothesis of pore throat effects as the possible cause of that phenomenon. Nevertheless, other effects (such as contact angle, wettability or network effects) can also contribute or justify hysteresis in porous media (Jury et al., 1991; Blunt et al., 2002; Spiteri et al., 2008). Note that when considering non-constrictive tubes ( $a = 1$ ) and  $R_{max} \gg R_{min}$ , it can be shown that the effective saturation and relative permeability expressions are similar to the ones of Brooks and Corey, and that the proposed permeability-porosity relationship is similar to that of Kozeny-Carman. Moreover, the presence of pore throats in the geometry allows the proposed model to describe media with high porosity and low permeability which cannot be properly represented with straight capillary tube models. Finally, if the constrictive and non-constrictive fractions of the pore have the same length ( $c = 0.5$ ), the proposed model is also consistent with the model derived by Guarracino et al. (2014) when considering the case of non-tortuous tubes ( $\tau = 1$ ).

516 The pore geometry modifies the macroscopic properties, porosity and permeability,  
517 through the factors  $f_v(a, c)$  and  $f_k(a, c)$  whose expressions differ for the sinusoidal and  
518 straight piecewise models. The influence of the model parameters  $a$  and  $c$  on the estimates  
519 of porosity and permeability has been tested by a sensitivity analysis. The results show  
520 that the most significant differences between the estimates of the models are obtained for  
521 low values of the length factor  $c$  over the entire range of the radial factor  $a$  values for both  
522 properties.

523 The estimates of effective saturation  $S_e$  and relative permeability  $k_{rel}$  have also been  
524 studied by a parametric analysis. It is important to remark that the main  $S_e$  and  $k_{rel}$   
525 drying and wetting curves have the same analytical expressions for both the sinusoidal and  
526 straight piecewise models. The expressions of those hydraulic properties are independent  
527 of  $c$  while depending on  $a$  that define the irregularities in the pore geometry. The results  
528 of the analysis show that the radial factor  $a$  controls the shape of the hysteretic loop  
529 (the distance between the drainage and imbibition curves), and in the limit case of  $a = 1$   
530 (straight tubes), the hysteresis disappears from the main curves as it will be expected.

531 The sinusoidal piecewise model is compared with experimental data from different  
532 soil textures. The estimates of hydraulic conductivity and water content as a function  
533 of the pressure head fit fairly well the data. In fact, the model is able to reproduce  
534 the behaviour of the data from the fitting of one set of parameters for both hydraulic  
535 properties simultaneously.

536 The models studied in this work provide relationships that estimate permeability as  
537 a function of porosity. The comparison with experimental data shows that these rela-  
538 tionships are satisfactorily able to reproduce the measured data over the entire range of  
539 porosities. Moreover, the agreements obtained for the sinusoidal and straight piecewise  
540 models are significantly better than the fit provided by the Kozeny-Carman equation.

541 The performance of the model to describe the hysteresis phenomenon present in the  
542 relative hydraulic properties is tested with experimental data sets of volumetric water  
543 content and pressure for drainage and imbibition experiments. The hysteretic behavior  
544 can be fairly reproduced by the model for two different sand textures. The comparison of  
545 the hysteretic loops for the two sands shows that the distance between the main drying  
546 and wetting curves is smaller for the finest texture. This result is consistent with the fitted  
547 values of the model parameters ( $a$  and  $D$ ) which are related to the pore-size distribution  
548 and geometry, and with the experimental measures of the soils properties from Yang et al.  
549 (2004).

550 The comparison between the sinusoidal and straight piecewise models shows that  
551 porosity and permeability are the most sensitive hydraulic properties to the pore geom-  
552 etry changes. Nevertheless, the relative properties, effective saturation and relative per-  
553 meability, present no variations for the same geometrical parameters of the models. The  
554 sinusoidal piecewise model represents an improvement over the straight piecewise model  
555 since its geometry is more similar to a real porous media due to the smooth changes be-  
556 tween the constrictive and non-constrictive lengths of the pore. Moreover, the sinusoidal  
557 piecewise model is a step forward in the geometry of capillary tube models whose key  
558 feature is to know the ratio between the pore throat radius and the pore radius. This

559 ratio is directly related to the radial factor  $a$ , and for a better characterization of a porous  
560 medium, it can be experimentally measured by applying the mercury injection method  
561 (Gao and Hu, 2013). Nonetheless, both studied models can be a valuable starting point  
562 to describe other physical phenomena that require hydraulic description at pore scale or  
563 accounting for the hysteresis phenomenon in the hydraulic properties and, therefore, en-  
564 hancing the possibility to a better understand of the processes that occur in the vadose  
565 zone.

## 566 6 Notation List

### 567 Declarations

568 **Funding:** Not applicable.

569 **Conflicts of interest/Competing interests:** The authors declare that they have no  
570 conflict of interest.

571 **Availability of data and material:** Not applicable. No original data, everything has  
572 been published before.

573 **Code availability:** Not applicable.

574 **Authors' contributions:** Conceptualization: MS, LG, DJ; Methodology: MS, LG, DJ;  
575 Writing-original draft preparation: MS, LG, DJ; Writing-review and editing: MS, LG,  
576 DJ; Investigation: MS, LG, DJ; Supervision: LG, DJ.

### 577 References

578 Bear, J., 1998. Dynamics of fluids in porous media. Dover Publications, Inc., Mineola,  
579 N.Y.

580 Blunt, M.J., Jackson, M.D., Piri, M., Valvatne, P.H., 2002. Detailed physics, predictive  
581 capabilities and macroscopic consequences for pore-network models of multiphase flow.  
582 Advances in Water Resources 25, 1069–1089.

583 Bodurtha, P., 2003. Novel techniques for investigating the permeation properties of  
584 environmentally-friendly paper coatings: The influence of structural anisotropy on fluid  
585 permeation in porous media. University of Plymouth.

586 Bousfield, D.W., Karles, G., 2004. Penetration into three-dimensional complex porous  
587 structures. Journal of colloid and interface science 270, 396–405.

588 Brooks, R.H., Corey, A.T., 1964. Hydraulic properties of porous media and their relation  
589 to drainage design. Transactions of the ASAE 7, 26–0028.

590 Bryant, S., Blunt, M., 1992. Prediction of relative permeability in simple porous media.  
591 Physical review A 46, 2004.

- 592 Buckingham, E., 1907. Studies on the movement of soil moisture. US Dept. Agric. Bur.  
593 Soils Bull. 38.
- 594 Burdine, N.T., 1953. Relative permeability calculations from pore size distribution data.  
595 Journal of Petroleum Technology 5, 71–78.
- 596 Cai, J., Chen, Y., Liu, Y., Li, S., Sun, C., 2022. Capillary imbibition and flow of wetting  
597 liquid in irregular capillaries: A 100-year review. Advances in Colloid and Interface  
598 Science , 102654.
- 599 Carman, P.C., 1937. Fluid flow through granular beds. Trans. Inst. Chem. Eng. 15,  
600 150–166.
- 601 Chen, K., Liang, F., Wang, C., 2021. A fractal hydraulic model for water retention and  
602 hydraulic conductivity considering adsorption and capillarity. Journal of Hydrology  
603 602, 126763.
- 604 Darcy, H., 1856. Exposition et application des principes à suivre et des formules à employer  
605 dans les questions de distribution d'eau. Les fontaines publiques de la ville de Dijon,  
606 Eds. Victor Dalmont, Paris 1856.
- 607 Dong, H., Blunt, M.J., 2009. Pore-network extraction from micro-computerized-  
608 tomography images. Physical review E 80, 036307.
- 609 Gao, Z., Hu, Q., 2013. Estimating permeability using median pore-throat radius obtained  
610 from mercury intrusion porosimetry. Journal of Geophysics and Engineering 10, 025014.
- 611 Guarracino, L., Rötting, T., Carrera, J., 2014. A fractal model to describe the evolution  
612 of multiphase flow properties during mineral dissolution. Advances in water resources  
613 67, 78–86.
- 614 Joekar-Niasar, V., Prodanović, M., Wildenschild, D., Hassanizadeh, S.M., 2010. Network  
615 model investigation of interfacial area, capillary pressure and saturation relationships  
616 in granular porous media. Water Resources Research 46.
- 617 Jougnot, D., Mendieta, A., Leroy, P., Maineult, A., 2019. Exploring the effect of the  
618 pore size distribution on the streaming potential generation in saturated porous media,  
619 insight from pore network simulations. Journal of Geophysical Research: Solid Earth  
620 124, 5315–5335.
- 621 Jury, W.A., Gardner, W.R., Gardner, W.H., 1991. Soil physics. John Wiley & Sons, Inc.  
622 New York .
- 623 Kozeny, J., 1927. Uber kapillare leitung der wasser in boden. Royal Academy of Science,  
624 Vienna, Proc. Class I 136, 271–306.

- 625 Lindquist, W.B., Venkatarangan, A., Dunsmuir, J., Wong, T.f., 2000. Pore and throat  
626 size distributions measured from synchrotron x-ray tomographic images of fontainebleau  
627 sandstones. *Journal of Geophysical Research: Solid Earth* 105, 21509–21527.
- 628 Man, H.N., Jing, X.D., 1999. Network modelling of wettability and pore geometry ef-  
629 fects on electrical resistivity and capillary pressure. *Journal of Petroleum Science and*  
630 *Engineering* 24, 255–267.
- 631 Mesri, G., Olson, R.E., 1971. Mechanisms controlling the permeability of clays. *Clays*  
632 *and Clay minerals* 19, 151–158.
- 633 Moebius, F., Or, D., 2012. Interfacial jumps and pressure bursts during fluid displacement  
634 in interacting irregular capillaries. *Journal of colloid and interface science* 377, 406–415.
- 635 Mualem, Y., 1976a. A catalog of the hydraulic properties of unsaturated soils. Research  
636 Project 442, Technion-Israel Inst. Technol., Haifa , 100p.
- 637 Mualem, Y., 1976b. A new model for predicting the hydraulic conductivity of unsaturated  
638 porous media. *Water resources research* 12, 513–522.
- 639 Mualem, Y., 1986. Hydraulic conductivity of unsaturated soils: prediction and formulas.  
640 *Methods of Soil Analysis: Part 1—Physical and Mineralogical Methods* , 799–823.
- 641 Oh, S., Kim, Y.K., Kim, J.W., 2015. A modified van genuchten-mualem model of hy-  
642 draulic conductivity in korean residual soils. *Water* 7, 5487–5502.
- 643 Or, D., Tuller, M., 1999. Liquid retention and interfacial area in variably saturated porous  
644 media: Upscaling from single-pore to sample-scale model. *Water Resources Research*  
645 35, 3591–3605.
- 646 Petersen, E.E., 1958. Diffusion in a pore of varying cross section. *AICHE Journal* 4,  
647 343–345.
- 648 Pham, H.Q., Fredlund, D.G., Barbour, S.L., 2005. A study of hysteresis models for  
649 soil-water characteristic curves. *Canadian Geotechnical Journal* 42, 1548–1568.
- 650 Reis, J.C., Acock, A.M., 1994. Permeability reduction models for the precipitation of  
651 inorganic solids in berea sandstone. *In situ* 18, 347–368.
- 652 Rembert, F., Jougnot, D., Guarracino, L., 2020. A fractal model for the electrical con-  
653 ductivity of water-saturated porous media during mineral precipitation-dissolution pro-  
654 cesses. *Advances in Water Resources* 145, 103742.
- 655 Soldi, M., Guarracino, L., Jougnot, D., 2017. A simple hysteretic constitutive model for  
656 unsaturated flow. *Transport in Porous Media* 120, 271–285.

- 657 Spiteri, E.J., Juanes, R., Blunt, M.J., Orr, F.M., et al., 2008. A new model of trapping  
658 and relative permeability hysteresis for all wettability characteristics. *Spe Journal* 13,  
659 277–288.
- 660 Stanić, F., Cui, Y.J., Delage, P., De Laure, E., Versini, P.A., Schertzer, D., Tchiguirin-  
661 skaia, I., 2020a. A device for the simultaneous determination of the water retention  
662 properties and the hydraulic conductivity function of an unsaturated coarse material;  
663 application to a green-roof volcanic substrate. *Geotechnical Testing Journal* 43.
- 664 Stanić, F., Delage, P., Tchiguirinskaia, I., Versini, P.A., Cui, Y.J., Schertzer, D., 2020b. A  
665 new fractal approach to account for capillary and adsorption phenomena in the water  
666 retention and transfer properties of unsaturated soils. *Water Resources Research* 56,  
667 e2020WR027808.
- 668 Thanh, L.D., Jougnot, D., Van Do, P., Van Nghia A, N., 2019. A physically based model  
669 for the electrical conductivity of water-saturated porous media. *Geophysical Journal*  
670 *International* 219, 866–876.
- 671 Topp, G.C., Miller, E.E., 1966. Hysteretic moisture characteristics and hydraulic conduc-  
672 tivities for glass-bead media. *Soil Science Society of America Journal* 30, 156–162.
- 673 Tuller, M., Or, D., Dudley, L.M., 1999. Adsorption and capillary condensation in porous  
674 media: Liquid retention and interfacial configurations in angular pores. *Water Re-*  
675 *sources Research* 35, 1949–1964.
- 676 Tyler, S.W., Wheatcraft, S.W., 1990. Fractal processes in soil water retention. *Water*  
677 *Resources Research* 26, 1047–1054.
- 678 Van Genuchten, M.T., 1980. A closed-form equation for predicting the hydraulic conduc-  
679 tivity of unsaturated soils. *Soil Sci. Soc. Am. J* 44, 892–898.
- 680 Vogel, H.J., Roth, K., 2001. Quantitative morphology and network representation of soil  
681 pore structure. *Advances in water resources* 24, 233–242.
- 682 Wang, S., Wu, T., Qi, H., Zheng, Q., Zheng, Q., 2015. A permeability model  
683 for power-law fluids in fractal porous media composed of arbitrary cross-section  
684 capillaries. *Physica A: Statistical Mechanics and its Applications* 437, 12–20,  
685 <https://doi.org/10.1016/j.physa.2015.05.089>.
- 686 Xu, C., Torres-Verdín, C., 2013. Pore system characterization and petrophysical rock  
687 classification using a bimodal gaussian density function. *Mathematical Geosciences* 45,  
688 753–771.
- 689 Xu, P., Zhang, L., Rao, B., Qiu, S., Shen, Y., Wang, M., 2020. A fractal scaling law  
690 between tortuosity and porosity in porous media. *Fractals* 28, 2050025.

- 691 Yang, H., Rahardjo, H., Leong, E.C., Fredlund, D.G., 2004. Factors affecting drying and  
692 wetting soil-water characteristic curves of sandy soils. *Canadian Geotechnical Journal*  
693 41, 908–920.
- 694 Yu, B., 2008. Analysis of flow in fractal porous media. *Applied Mechanics Reviews* 61,  
695 050801.
- 696 Yu, B., Lee, L.J., Cao, H., 2002. A fractal in-plane permeability model for fabrics. *Polymer*  
697 *composites* 23, 201–221.
- 698 Yu, B., Li, J., 2001. Some fractal characters of porous media. *Fractals* 9, 365–372.
- 699 Yu, B., Li, J., Li, Z., Zou, M., 2003. Permeabilities of unsaturated fractal porous media.  
700 *International journal of multiphase flow* 29, 1625–1642.

Symbol	Description	Units
REV	Representative elementary volume	-
$R$	Radius of a circular tube	m
$a$	Radial factor of the constrictivity	-
$c$	Length factor of the constrictivity	-
$\lambda$	Wavelength	m
$l$	Pore length	m
$r(x)$	Pore radius variation along the longitudinal variable $x$	m
$M$	Integer number	-
$V_p$	Pore volume	m <sup>3</sup>
$f_v$	Reduction factor in a pore volume and in the porosity	-
$q_p$	Pore volumetric water flow	m <sup>3</sup> s <sup>-1</sup>
$\Delta h$	Pressure head drop	m
$f_k$	Reduction factor in a pore volumetric water flow and in the permeability	-
$R_{REV}$	REV radius	m
$L$	REV length	m
$\tau$	Tortuosity	-
$N(R)$	Number of pores of radius equal or larger than $R$	-
$D$	Fractal dimension	-
$R_{min}$	Minimum pore radius	m
$R_{max}$	Maximum pore radius	m
$\phi$	Porosity	-
$q$	Volumetric water flow through the REV	m <sup>3</sup> s <sup>-1</sup>
$k$	Permeability	m <sup>2</sup>
$k_{rel}$	Relative permeability	-
$h$	Pressure head	m
$T_s$	Surface tension	N m <sup>-1</sup>
$\beta$	Contact angle	degrees
$S_e$	Effective saturation	-
$S_e^d, S_e^w$	Main drying and wetting effective saturation, respectively	-
$h_{min}$	Minimum pressure head	m
$h_{max}$	Maximum pressure head	m
$k_{rel}^d, k_{rel}^w$	Main drying and wetting relative permeability, respectively	-
$\rho$	Water density	kg m <sup>-3</sup>
$g$	Gravity	m s <sup>-2</sup>
$\mu$	Water dynamic viscosity	Pa s